UAM
Universidad Autónoma de Madrid

Biblos-e Archivo
Repositorio Institucional UAM

Repositorio Institucional de la Universidad Autónoma de Madrid
https://repositorio.uam.es

Esta es la **versión de autor** del artículo publicado en:
This is an **author produced version** of a paper published in:

Chemical Engineering Journal 397 (2020): 125479

DOI: https://doi.org/10.1016/j.cej.2020.125479

Copyright: © 2020 Elsevier B.V. This manuscript version is made available under the CC-BY-NC-ND 4.0 licence http://creativecommons.org/licenses/by-nc-nd/4.0/

El acceso a la versión del editor puede requerir la suscripción del recurso
Access to the published version may require subscription

Deactivation and regeneration of activated carbon-supported Rh and Ru catalysts in the hydrodechlorination of chloromethanes into light olefins

Maria Martin-Martinez[a,], Juan J. Rodriguez[a], Richard T. Baker[b], Luisa M. Gómez-Sainero[a]*

[a]Departamento de Ingeniería Química, Facultad de Ciencias, Universidad Autónoma de Madrid, Cantoblanco, 28049 Madrid, Spain

[b]School of Chemistry, University of St Andrews, North Haugh, St Andrews, Fife KY16 9ST, United Kingdom

*CORRESPONDING AUTHOR:

e-mail: maria.martin.martinez@uam.es

Tel: +34 91 497 5527

Fax: +34 91 497 3516

Abstract

This work analyses the deactivation of activated carbon-supported Rh and Ru (both at 1 *wt.*%) catalysts (Rh/C and Ru/C) in the hydrodechlorination (HDC) of dichloromethane (DCM) and chloroform (TCM). The deactivation can be mainly attributed to the coverage of active metal centres by organometallic species resulting from the chemisorption of reaction products, such as olefins, at the electro-deficient metal sites. With DCM, the activity of Ru/C decreased by more than 80% after 90 h on stream at 250 °C and with a space time of 1.7 kg h mol^{-1}. Under the same conditions, with TCM, the Rh/C and Ru/C catalysts lost 75% of activity after 84 and 54 h on stream, respectively. A regeneration treatment with air at 250 °C allowed complete recovery of the catalytic activity. After each deactivation-regeneration cycle, the selectivity to olefins increased. Therefore, HDC with the catalysts tested provides a promising way for the upgrading of chloromethanes from waste gas streams into light olefins.

Keywords: Hydrodechlorination; Olefins; Rh/C; Ru/C; Deactivation; Regeneration

1. Introduction

Dichloromethane (DCM) and chloroform (TCM) are harmful pollutants which can be found in waste gas streams from chemical and pharmaceutical industries, since they are widely used as solvents, for printing, dry cleaning, synthesis of adhesives, pesticides, pharmaceutical products or refrigerants [1]. The European Parliament (Regulation (EC) No 166/2006) establishes emission limits to air of 1000 kg/year and 500 kg/year for DCM and TCM, respectively [2]. Besides, maximum exposure limits in air for an 8-hour workday as low as 25 ppm of DCM [3] and 50 ppm of TCM [4] have been recommended.

Since the release of these chloromethanes into the environment is subject to strict legal regulations, several technologies are being developed for their abatement. Hydrodechlorination (HDC) is a reductive treatment which operates at close to atmospheric pressure and relatively low temperatures, with the help of an appropriate catalyst, to transform these chlorinated pollutants into harmless chlorine-free hydrocarbons that could be recycled for chemical or energy applications [5, 6]. The main problem in HDC is catalyst deactivation, a crucial issue for the potential application of this technology. However, this problem has been barely addressed in the literature. The HCl produced upon HDC has been identified as a common catalyst deactivation agent in this process [7-11]. This byproduct can be adsorbed on the catalyst, favoring coke formation, with consequent deactivation by partial blockage of the active surface [10, 12-14]. Electronic transformations may also occur in the catalysts, giving rise to changes in the oxidation state of the active metallic phase and/or in the nature of surface groups [17]. Another common cause of deactivation is the sintering of the active phase when higher temperatures are used to enhance catalyst activity [18-20].

In previous studies, the gas phase HDC of DCM and TCM was investigated using different metallic catalysts supported on activated carbon (Pt/C, Pd/C, Rh/C and Ru/C) [21-23]. While Pt/C yielded mainly methane and exhibited excellent stability [23, 25], the other three catalysts gave rise to significant relative amounts of higher hydrocarbons of more industrial interest, but suffered deactivation to different extents [21, 22]. It is important to understand the causes of these two different behaviors in order to enable the design of improved catalysts for HDC. In addition, because of the different selectivities observed, sometimes it is more convenient to use a specific catalyst in spite of it being less stable, and then investigate some suitable way of regenerating it. Deactivation of Pd/C has been widely studied [17, 22], being mainly attributed to the formation of a new

PdC_x phase, promoted by the HCl produced (in HDC of DCM), or to metal sintering (in HDC of TCM). However, despite suffering the greatest loss of activity, the causes of deactivation of Rh/C and Ru/C catalysts during HDC have not been clarified so far. Rh/C has shown a good ability for the production of valuable olefins and hydrocarbons higher than methane by HDC of chloromethanes [25]. Therefore, it is important to understand its deactivation and to design a method for its regeneration.

The regeneration of catalysts used in HDC has been scarcely investigated in the literature, and mainly for Pd-based catalysts. Two different strategies have been followed: (i) *in situ* gas flow methods, and (ii) washing methods. Among the first, O_2, air or inert gas flows at different temperatures have been used to remove carbonaceous deposits or coke [26, 27]. In a recent study, we used air at 250 °C to successfully regenerate a Pd/C catalyst deactivated by PdC_x [17]. On the other hand, H_2 flow has been found to be useful for the removal of deactivating chlorine species [26, 27]. Other authors have combined oxidation and reduction steps for regenerating HDC catalysts [28-31]. Among the washing methods, NaOH and ammonia have been found to be suitable agents for the regeneration of different Pd, Pd-Pt and Pd-Rh catalysts deactivated by the deposition of different compounds [30, 32].

The objectives of the current work are to elucidate the deactivation of Rh/C and Ru/C catalysts during the HDC of DCM and TCM, and then to find a feasible regeneration treatment.

2. Experimental

2.1. Catalysts preparation

Carbon-supported Rh and Ru catalysts were prepared by incipient wetness impregnation of a commercial activated carbon (*Erkimia S.A.*, the fraction with a particle size between 0.25 and 0.50 mm), whose description has been reported elsewhere [22], using aqueous solutions containing the appropriate amounts of either $RhCl_3$ or $RuCl_3$ (supplied by *Sigma-Aldrich*) to give a final metal loading of 1 wt%. After drying overnight at room temperature, followed by heating at 100 °C for 2 h (heating rate: 20 °C h^{-1}), the catalysts were activated by reduction under continuous H_2 flow (50 ml min^{-1}) at 250 °C for 2 h (10 °C min^{-1}). Hydrogen was supplied by *Praxair* with a minimum purity of 99.999%. The as-prepared catalysts (in all cases reduced at 250 °C) were named Rh/C and Ru/C.

2.2 Catalysts characterization

The surface composition of the catalysts was analyzed by X-ray photoelectron spectroscopy (XPS) with a *5700C Multitechnique System (Physical Electronics*), using Mg-Kα (1253.6 eV) radiation, scanning up to a binding energy (BE) of 1200 eV for the determination of the elements present and their concentrations (general spectra). The C 1s peak (284.8 eV) was employed as an internal standard to correct the shift in BE caused by sample charging. The BE of the C 1s, O 1s, Cl 2p, Rh 3d and Ru 3d core levels and the full width at half maximum values were used to assess the chemical state of the elements at the catalyst surface (partial spectra). The peaks were deconvoluted according to literature procedures, by using mixed Gaussian–Lorentzian functions and a least-squares method [33]. The X-ray diffraction (XRD) patterns of the catalysts were obtained in an *X'Pert PRO Panalytical* diffractometer, using Cu Kα monochromatic radiation (of wavelength 0.154056 nm), a 2θ scanning range of 10° to 100° and a scan step size of 0.04°. Scanning Electron Microscopy (SEM) images were obtained using a *Jeol 6700F*

instrument with Field Emission Gun, in back-scattered electron mode, where the intensity is related approximately to the square of the average atomic number at each point of the image. This allows compositional information to be obtained since phases of different densities may be distinguished. An accelerating voltage of 15 kV and a working distance of 8.6 mm were used. Transmission electron microscopy (TEM) images were obtained using *Jeol JEM 2011* and *Jeol JEM 2100* instruments, operating with a LaB_6 filament at an accelerating voltage of 200 kV (0.18 nm point resolution), both equipped with an EDS unit (*Oxford INCA*) and a *Gatan* (in *Jeol JEM 2011*) or *Orius SC1000* (in *Jeol JEM 2100*) CCD camera. The samples for TEM were ground, suspended in ethanol and deposited onto holey carbon-coated Cu grids. Thermogravimetric analysis (TGA) were performed using a *TGA Q-500* thermo-balance. Powder samples were heated at 10 °C min^{-1} up to 900 °C in both air and nitrogen atmospheres. N_2 adsorption-desorption isotherms at -196 °C were obtained using a *Tristar II 3020 (Micromeritics)* to characterize the porous structure of the catalysts. The samples were previously outgassed for 12 h at 150 ºC at a residual pressure of 10^{-3} Torr (*VacPrep 061, Micromeritics*). The specific surface areas (S_{BET}) were calculated using the BET equation and the t-method was used to obtain the micropore volume (V_{micro}).

2.3. Hydrodechlorination experiments

The activity of the catalysts in the HDC was evaluated in a continuous flow reaction system (*Microactivity Pro, PID Eng & Tech*) equipped with a quartz fixed bed micro-reactor (internal diameter 0.95 cm). The analysis of the reaction products was performed using a gas chromatograph (*CP-3800, Varian*), equipped with a flame ionization detector (FID) and a 60 m capillary column (*CP-Silica Plot, Varian*), coupled on-line to the reactor. Long-term (90 h) experiments were performed to examine the evolution of the catalytic activity as a function of time on stream. The experiments were performed at

atmospheric pressure, using a total gas flow rate of 100 Ncm^3 min^{-1}, a H_2/chloromethane (CM) molar ratio of 100, a reaction temperature of 250 °C and a space-time (τ, ratio between the mass of catalyst used and the CM molar flow) of 1.7 kg h mol^{-1}. The gas feed, with a CM concentration of 1000 ppmv, was prepared by mixing the commercial CM/N_2 starting mixture with N_2 (both supplied by *Praxair*) in the appropriate ratios. Mass transfer limitations were experimentally determined by means of a series of experiments in which the total flow rate and the catalyst particle size were varied. No significant changes in activity were observed within the ranges of 0.02–0.06 m s^{-1} for gas velocity and 0.25-0.71 mm for particle size [34]. The behavior of the catalysts was evaluated in terms of overall CM dechlorination, CM conversion, and selectivity to the different reaction products. The experimental results were reproducible with less than 5% error.

2.4. Catalysts regeneration

A second set of experiments was carried out to study the reusability of the catalysts after regeneration, operating as described in section 2.3. First, the catalysts were used during a 90 h HDC experiment (at atmospheric pressure, with total gas flow rate of 100 Ncm^3 min^{-1}, CM concentration of 1000 ppmv, H_2/CM molar ratio of 100, space time of 1.2 kg h mol^{-1} and a reaction temperature of 250 °C). The resultant deactivated catalysts were regenerated at atmospheric pressure by flowing 50 Ncm^3 min^{-1} of air (supplied by *Praxair*) into the system at 250 °C for 12 h. The activity of the catalysts was studied over three consecutive deactivation-regeneration cycles.

3. Results and Discussion

3.1. Catalytic activity

Figure 1 shows the evolution of DCM conversion, selectivity to reaction products and global dechlorination during time on stream when using the Rh/C and Ru/C catalysts. Figure 2 presents the analogous results for the HDC of TCM. As can be observed, at the experimental conditions used, both catalysts showed high initial activities but different deactivation and selectivity patterns thereafter. Both catalysts suffered a dramatic deactivation with time on stream during the HDC of TCM, where Rh/C and Ru/C lost 75% of their initial activity in 84 h and 54 h, respectively. On the other hand, in the HDC of DCM, Rh/C had lost only 15% of its activity after 90 h, whereas the Ru/C suffered a rapid deactivation in the same time period (82% in 90 h).

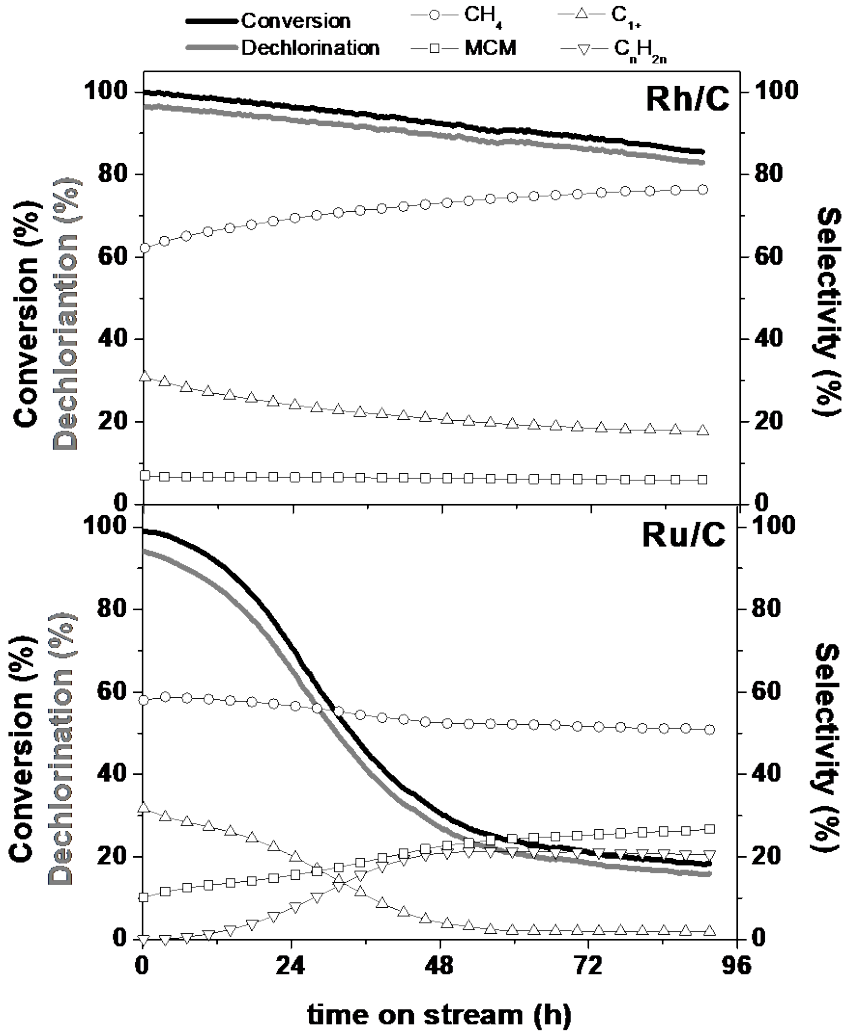

FIGURE 1. Evolution of the activity, selectivity to reaction products and overall dechlorination during time on stream in the HDC of DCM with Rh/C (top) and Ru/C (bottom).

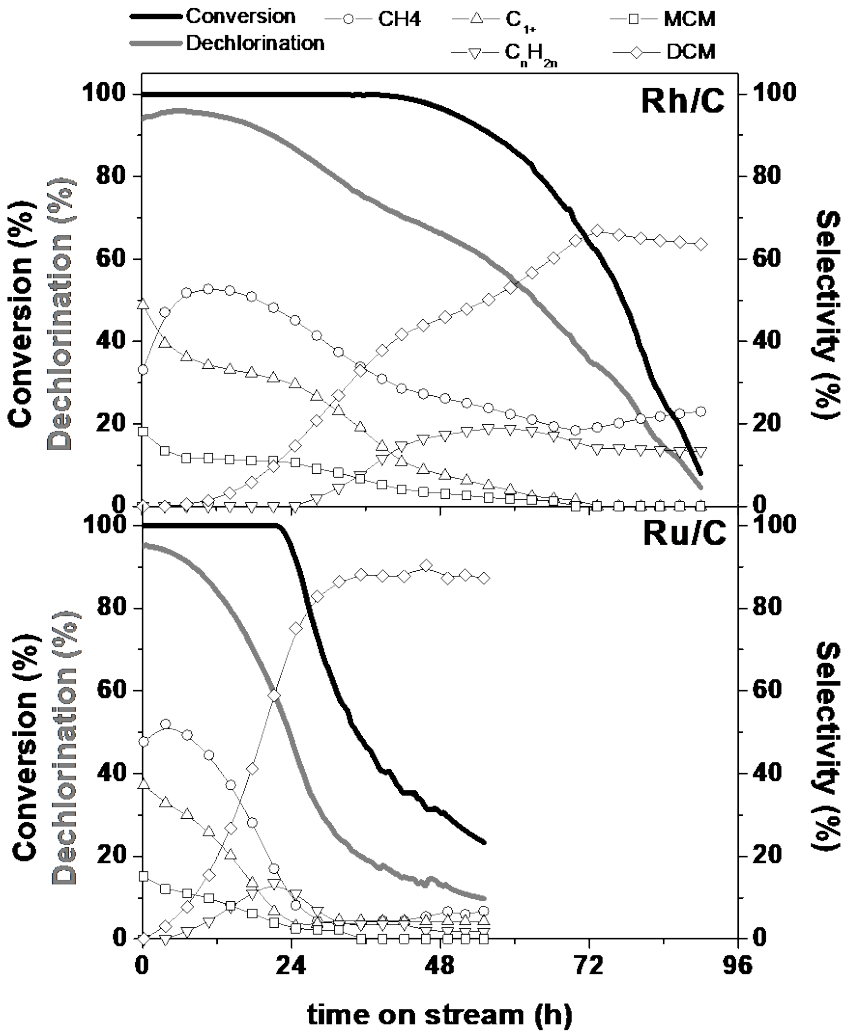

FIGURE 2. Evolution of the activity, selectivity to reaction products and overall dechlorination during time on stream in the HDC of TCM with Rh/C (top) and Ru/C (bottom).

The variability of selectivity to reaction products as a function of time on stream suggests important changes occur in the nature of the active centers during catalyst operation, particularly in the HDC of TCM. In this reaction, in the first hours of operation, an increase in the selectivity to olefins (C_nH_{2n}) and DCM can be observed with both catalysts, at the expense of alkanes (CH_4 and C_{1+}) and MCM. Nevertheless, when the catalyst deactivation becomes significant, the selectivity to olefins decreases again in both cases. An increase in the production of olefins with time on stream was also observed in the HDC of DCM when using the Ru/C catalyst, this time coupled with an increase in

MCM, against a decreasing selectivity to alkanes. In contrast, when Rh/C was employed in the HDC of DCM - the catalyst that suffered the least deactivation - much smaller variations are observed in the selectivities with time on stream; the selectivity to methane increasing slightly at the expense of that to the higher alkanes (C_{1+}). All the observed changes in the selectivity patterns of the catalysts may be caused by changes in the nature of the active centers occurring during catalyst operation. It is also clear that the dechlorination capabilities of both Rh/C and Ru/C were poorer in the HDC of TCM than of DCM, due to the higher concentrations of hydrogen needed for the total substitution of the chlorine atoms in TCM (three atoms) than in DCM (two atoms). The higher reactivity of the former makes this effect even more significant.

3.2. Characterization of the catalysts

In order to understand the differences in the catalysts activity observed, the physical and chemical properties of the catalysts were studied and compared before and after used in the dechlorination reactions. This will allow understanding the changes in the nature of the active centers that were suggested by the variability of selectivity with time on stream.

3.2.1. Bulk metal content, specific surface area and metal dispersion

The values of bulk metal content (M_{bulk}), specific surface area (S_{BET}) and metal dispersion (D) of the catalysts as prepared and after the long-term experiments of Figures 1 (U_{DCM}) and 2 (U_{TCM}) were reported in a previous study [21] and are summarized in Table S1 of the Supplementary Information. Briefly, the bulk metal content does not vary during HDC. CO chemisorption results showed that the active metal phase in the synthesized catalysts were undoubtedly well dispersed, but that a significant loss of accessible active phase was observed after their use in HDC. This was especially pronounced in the case of Ru/C for both reactions, and Rh/C in the HDC of TCM. This is consistent with the fact

that these cases were the ones in which the highest loss of activity was observed. Finally, both catalysts showed high initial BET surface area, *ca.* 1100 m^2 g^{-1}, which sharply diminished after the HDC of TCM, evidencing a severe blockage of the pore structure, which would explain their rapid deactivation. The blockage by carbonaceous deposits - sometimes including chlorine in its composition - has been reported in HDC by other authors [8, 10, 30, 35]. First, coke (mainly composed of polymerized hydrocarbons) may accumulate due to decomposition or condensation of hydrocarbons in the catalyst surface [36]. On the other hand, the HCl, or other chlorinated byproducts released during the reaction, may modify the oxidation state of the active phase, generating new electro-deficient active centres. Consequently, besides the typical products obtained in the HDC, oligomers may be produced and deposited on the catalyst surface during the reaction [36].

3.2.2. X-ray photoelectron spectroscopy

Table 1 shows the elemental surface composition of the catalysts as prepared and after use in the HDC of DCM (U_{DCM}) and TCM (U_{TCM}). The catalysts mainly present C (88-95 %) and O (3-8 %) on their surfaces. In the catalysts prepared with Rh, this metal is the next most abundant element at the surface. However, the catalysts prepared with Ru showed none of this metal by XPS, revealing its preference to deposit in the internal pores of the support, which can be ascribed to a strong interaction between the Ru particles and the support, as was previously reported for a Ru/C catalyst by Álvarez-Montero et al. [37]. The different behaviour of Rh/C in the HDC of DCM (no dramatic loss of dispersion and smooth deactivation) may be related to the migration of the Rh species to the catalyst surface, as suggested by the increase in surface Rh concentration observed after the HDC of DCM (Table 1). It should be noted that the surface concentration of Cl increases significantly after the reaction, especially in the HDC of TCM.

TABLE 1. Data obtained from XPS spectra for the catalysts as-prepared and after use in DCM (U_{DCM}) and TCM (U_{TCM}): surface compositions as elemental atomic concentrations and quantification of the chemical states of each element at the surface by deconvolution of M (Rh/Ru) 3d, Cl 2p, C 1s and O 1s regions.

(%)		Rh/C	Rh/C U_{DCM}	Rh/C U_{TCM}	Ru/C	Ru/C U_{DCM}	Ru/C U_{TCM}
atomic concentration	C	89.95	88.15	89.22	94.88	94.56	93.88
	N	1.07	1.19	0.65	0.84	0.60	0.39
	O	6.87	7.95	2.96	4.12	4.62	3.35
	Cl	0.38	0.51	5.38	0.16	0.21	2.38
	M	1.72	2.19	1.80	-	-	-
M (3d)	M^0	17.1	21.2	43.5	-	-	-
	M^{n+}	82.9	78.8	56.5	-	-	-
Cl (2p)	$Cl_{inorg.}$	54.9	48.5	4.7	18.7	7.2	1.2
	$Cl_{org.}$	45.1	51.5	95.3	81.3	92.8	98.8
C (1s)	C=C	55.1	63.7	79.0	58.4	64.2	71.7
	C-C	28.3	22.7	10.7	24.6	22.0	15.7
	C-O	9.7	7.3	7.1	10.2	7.2	8.3
	C=O	7.0	6.3	3.2	6.8	6.6	4.3
O (1s)	C=O	53.7	50.1	32.9	49.8	36.9	36.6
	C-O	32.8	46.9	64.8	47.3	57.8	58.7
	O_{ads}	13.5	3.0	2.4	2.9	5.3	4.8

According to literature [38-40], the XPS signal for the Rh $3d_{5/2}$ orbital may be deconvoluted into three species, centred at 307.8 eV (corresponding to zero-valent Rh^0), 309.2 eV (electro-deficient Rh^{n+}) and 311.2 eV (satellite of Rh^{n+}), with their corresponding doublet peaks for the Rh $3d_{3/2}$ orbital at 312.5 eV (Rh^0), 313.9 eV (Rh^{n+}) and 115.9 eV (Rh^{n+}) (see Figure S1 of Supplementary Information). In addition, the signal for the Cl 2p orbital may be also deconvoluted into three features, centred at 198 eV (inorganic Cl), 200 eV (organic Cl) and 202 eV (organic Cl). As can be seen in Table 1, the total amount of Rh^{n+} species decreases after the HDC, evidencing the selective poisoning of the electro-deficient sites, whilst the proportion of organic chlorine (Cl_{org}) increases. This suggests that chlorinated organic compounds are being deposited on the Rh^{n+} species of the catalysts, so explaining the increase observed in surface chlorine

concentration. What is more, after the HDC of TCM, the Rh peaks shift to lower binding energies, especially the peaks related to Rh^{n+} (Rh peaks appear at 307.6, 308.6 and 310.8, respectively) (Figure S1). This suggests structural changes are occurring, particularly in the Rh^{n+} species, probably due to the formation of new bonds with the reactants and/or the reaction products formed during the HDC of TCM. Rh can exist in several oxidation states, being able to form many different organometallic Rh complexes. Due to the previously-reported efficiency of Rh/C to produce olefins by HDC [25], it seems plausible that $[RhCl(C_2H_4)]_2$ or $[RhCl(C_2H_4)_2]_2$ olefinic complexes are being formed [41-43]. Moreover, the named study [25] pointed out the high-energy barrier needed for olefin desorption from Rh active sites, in contrast to the low adsorption energy, which supports its likely contribution to catalyst poisoning.

For the Ru catalysts, XPS data on Cl content and chemical state showed the higher proportion of organic chlorine in all cases, close to 100 % for the used samples. This points to a similar deactivation mechanism in the Ru/C catalyst as that discussed above for Rh/C, were chlorinated organic compounds are deposited on the active phase of the catalysts. The formation of heavy halogenated carbonaceous deposits has been reported previously as the main cause of deactivation for Ru/C catalysts used in HDC [44].

Table 1 also provides information on the different functional groups identified by deconvolution of the C 1s and O 1s regions of the XPS spectra. For C 1s, four signals were observed: (1) the peak at BE ~284.8 eV is attributed to the C=C bonds (sp^2 structures); (2) at BE ~285.8 eV, the peak is assigned to C–C (sp^3 carbon species); (3) BE ~287.7 eV corresponds to C–O (epoxy and hydroxyl groups); and (4) BE ~290.7 eV is attributed to C=O (carbonyl, carboxyl and carboxylate groups) [45]. On the other hand, the O1s spectra show the presence of three different components: (1) BE ~531.4 eV is assigned to C=O (carbonyl and carboxyl groups); (2) BE ~533.3 eV corresponds to C–O

(phenolic, ether and hydroxyl groups); and (3) BE ~535.5 eV is attributed to adsorbed atomic O [45]. Considering the C_{1s} region, both catalysts show very similar initial surface carbon compositions, with *ca.* 55 % as unsaturated C=C, *ca.* 25 % as C-C and *ca.* 20 % as oxygenated species. After the HDC there is an increase in the surface concentration of sp^2 structures, especially in the catalysts used in TCM, which supports the hypothesis of the chemisorption of olefins suggested before. Looking now at the O_{1s} region, the proportion of oxygenated C=O groups decreases in favour of other oxygenated phenolic/hydroxyl and ether groups. This can be attributed to the reducing environment experienced by the catalysts during the HDC.

3.2.3. X-ray diffraction

Figure 3 shows the XRD profiles of the catalysts as prepared and after use in HDC (U_{DCM}, U_{TCM}). There are no peaks attributable to Rh in any of the diffractograms. However, after using Ru/C in the HDC of DCM, two peaks were observed at 40° and 46.4°, corresponding to different Ru-containing phases. These peaks did not appear in the catalysts before the reaction, indicating that Ru particles increased in size during the HDC, in agreement with the strong decrease of dispersion, from 20% to 2%, observed previously. Moreover, these peaks appear at values of 2θ *ca.* 2° higher than is typical for metallic Ru, implying a decrease of its lattice parameter, which may be caused by the generation of new stronger bonds formed with different elements during the reaction, probably due to the formation of new organochlorinated Ru complexes. The peaks appearing at 36.8° in Rh/C and 36.1° in Ru/C match to the corresponding metallic chlorides (according to Powder Diffraction Files References 96-153-4199 and 96-153-5288, respectively). Under the reducing environment of the HDC experiments, these peaks decrease in size, although they do not completely disappear, and a peak at *ca.* 35.5°

appears, which may be related to a new organometallic phase, for each metal, containing chlorine, and even other heteroatoms like oxygen (coming from the surface of the support), produced from the chemisorption of reactants and reaction products on the M^{n+} species of the catalysts. This reflection has been reported before for several chlorinated Rh and Ru organometallic complexes, *e.g.* $Rh_8Cl_8O_8H_{224}C_{136}$ [46], $Rh_4Cl_4C_{84}H_{80}$ [47], $Rh_2Cl_2N_4C_{34}H_{56}$ [48], $Rh_4Cl_8N_8O_{16}C_{104}H_{156}$ [49], $Ru_4Cl_4C_{48}H_{68}O_8$ [50], $Ru_2Cl_4O_2N_4C_{70}H_{80}$ [51].

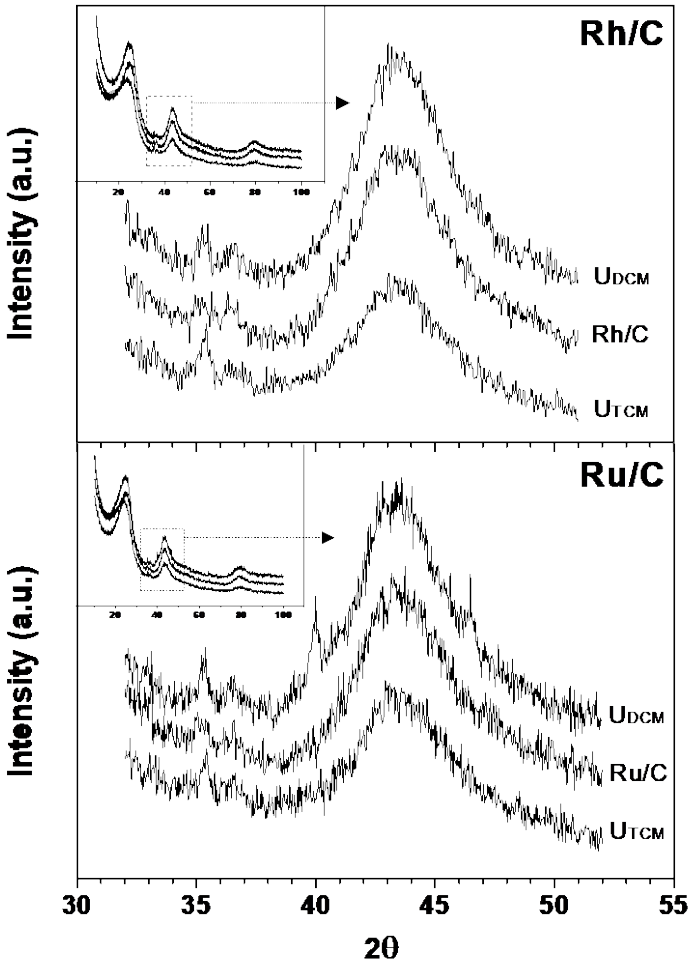

FIGURE 3. XRD profiles of the Rh/C and Ru/C catalysts as prepared and after use in the HDC of DCM and TCM.

3.2.4. Electron microscopy

Figure 4 shows TEM and SEM images of Rh/C before and after the HDC of DCM and TCM. As was presented in Table S1, the Rh/C catalyst possesses the highest metal dispersion (32 %). The comparison between the bulk Rh content (from Table S1) and the surface Rh concentration (by XPS, Table 1), indicates that Rh particles are mainly deposited on the outer surface of the catalyst (when expressed as atomic concentrations, $Rh_{XPS}/Rh_{bulk} \approx 18$). Nevertheless, these particles were difficult to find even by SEM, probably due to their small sizes (Figure 4a). On the other hand, the high proportion of Rh in an electro-deficient state detected by XPS, perhaps present in the form of $RhCl_3$, as suggested by XRD, appears to result in the irregularly-shaped Rh particles detected in TEM (Figure 4b). According to temperature programmed reduction results (TPR) from a previous study [37], at the reduction temperature used, the catalyst should be completely reduced. However, in the prepared catalyst (reduced at 250 °C), both reduced Rh^0 and electro-deficient Rh^{n+} species are detected by XPS (Table 1, Figure S1). This suggests that Rh^{n+} are not unreduced species. What is more, reduction temperatures of up to 450 °C were employed in a recent study of this catalyst, but no significant differences were found either in the Rh^0/Rh^{n+} ratio or in the metal dispersion, over the range of reduction temperatures studied (250-450 °C) [23]. The mean particle size calculated for this catalyst is 1.3 nm. After the catalyst was used in the HDC of DCM the mean particle size increased to 6.8 nm, with an observed size range of about 2 to 14 nm (Figure 4c). Particles were also imaged in the catalyst used in the HDC of TCM (Figure 4d), and these had a mean particle size of 5.3 nm. Their EDS analysis reveals a significant amount of Cl, which is in agreement with the XRD and XPS results presented above.

Turning now to the Ru/C catalyst (Figure 5), since the Ru particles are mainly located in the interior of the support particles, it was not possible to detect them by SEM. Therefore,

only TEM images are shown here. The images of the as prepared catalyst show a large number of round Ru particles of around 2 nm diameter (Figure 5a), but also bigger Ru clusters (up to 14 nm) in which large amounts of Cl were detected by EDS (Figure 5b) and attributed to the precursor used in the catalyst synthesis ($RuCl_3$). The TPR profile of Ru/C presented in a previous study [37] showed three peaks of H_2 consumption at 114, 184 and 248 °C, attributed to the reduction of different precursor phases [52]. This could explain the presence of Ru-Cl-C clusters in the catalyst. The mean Ru particle size found for this catalyst, including these clusters, is 3.3 nm. The catalyst used in the HDC of DCM (Figure 5c) also contain rounded particles, but bigger in size, with a mean particle size of 10.9 nm, over a detected range of 5.7 to 24 nm, in agreement with the XRD (Figure 3) and chemisorption (Table S1) results presented above. For the catalyst used in the HDC of TCM (Figures 5d and 5e), finding well-defined particles was a challenge. Figure 5e presents a particle of 2 nm, showing interplanar spacings of 2.31 Å (±0.05 Å), consistent with the (100) planes of the hexagonal close packed Ru structure. The EDS analysis of selected areas reveals the presence of large amounts of Cl (Figure 5d), supporting the hypothesis concerning the poisoning of the active sites by organochlorine species.

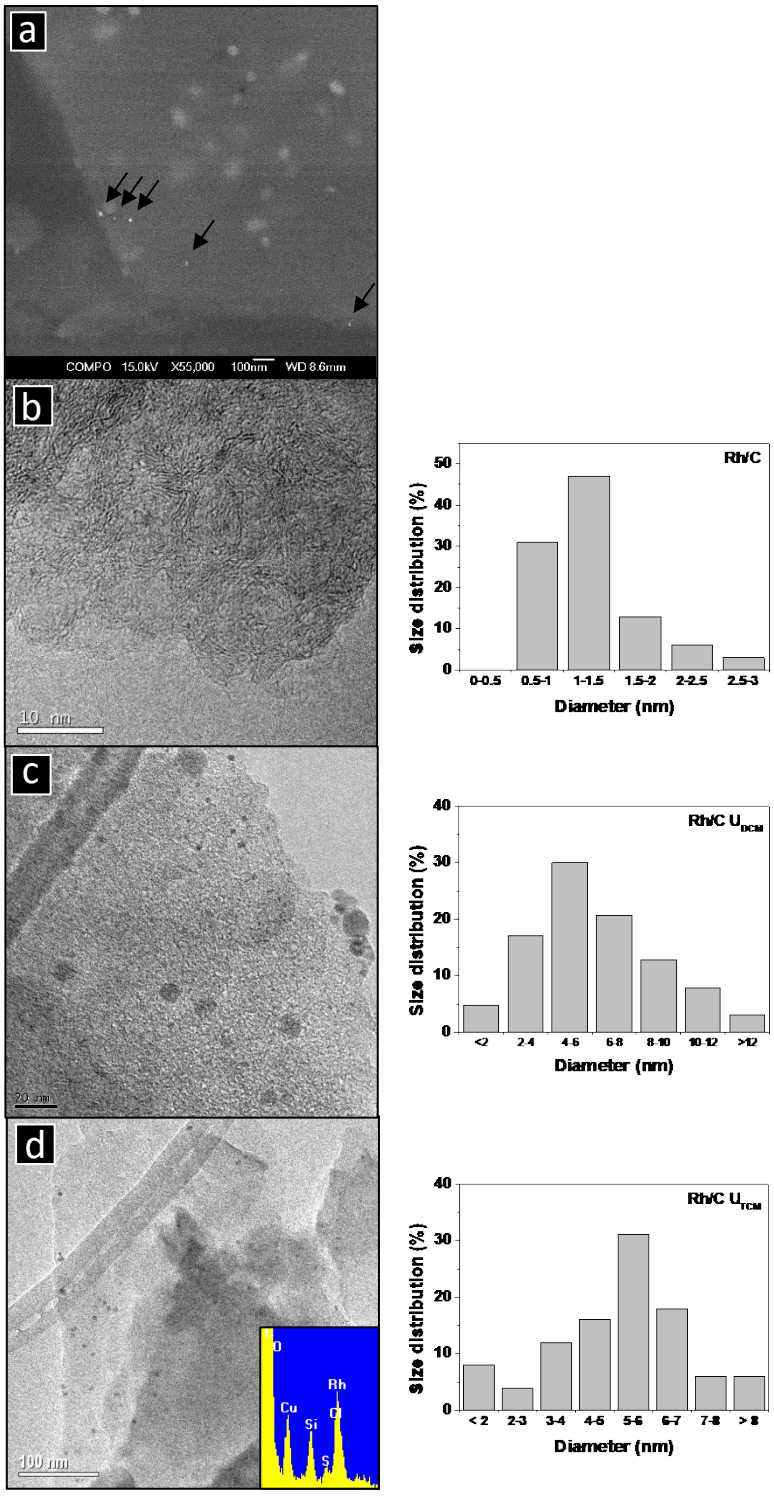

FIGURE 4. FEG-SEM (a) and TEM (b-d) images of the Rh/C catalyst before (a,b) and after the HDC of DCM (c) and TCM (d) with corresponding metal particle size distribution histograms.

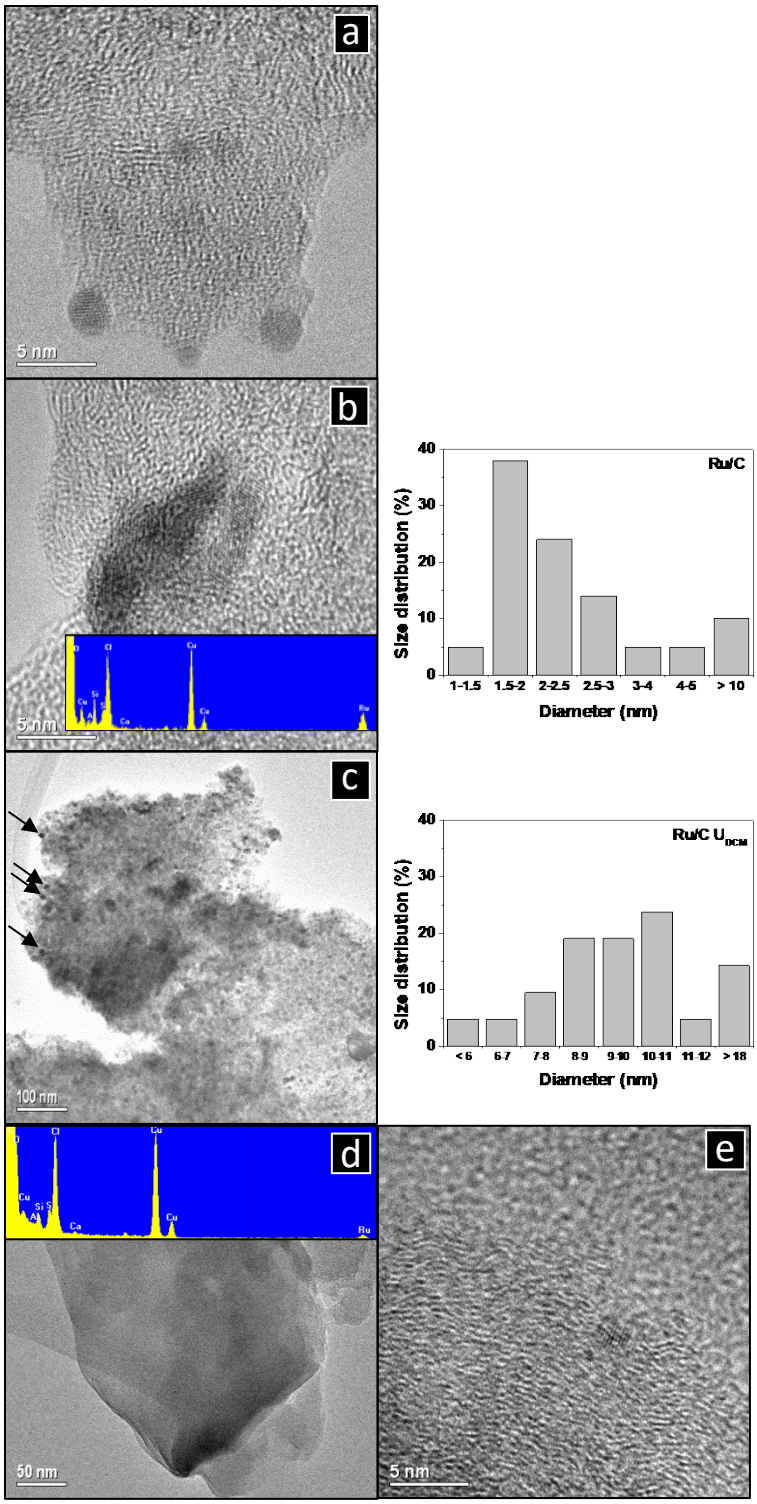

FIGURE 5. TEM images of the Ru/C catalyst before (a,b) and after the HDC of DCM (c) and TCM (d,e), with particle size distribution histograms.

3.2.5. Thermogravimetry

Figures 6 and 7 present the TGA spectra of Rh/C and Ru/C, before and after the HDC reactions, obtained under oxidizing (Air) and inert (N_2) atmospheres, respectively. Figure 6 shows significant weight loss at temperatures above 400 °C, corresponding to the combustion of the activated carbon itself. At the end of each TGA run in air, a small mass remains, which is related to the ash content of each catalyst, around 6% in all the cases. The weight losses observed in the experiments under inert atmosphere (Figure 7) correspond mainly to the decomposition of the compounds adsorbed on the catalysts. As can be seen, the weight loss detected in the used catalysts at temperatures below 500 °C is considerably greater than that observed in the reduced catalysts, especially in the samples used in the HDC of TCM. The oligomerization of the (chlorinated) compounds chemisorbed on the active sites might be more favourable when treating TCM than DCM, due to the higher amount of chlorine available in the former. This is consistent with the sharp drop in the BET area observed in the catalysts after the HDC of TCM (Table S1). On the other hand, when the gas released in each TGA run is analysed with a mass spectrometer and the mass/charge ratios (m/e) examined, a large number of signals characteristic of the decomposition of hydrocarbons are detected. The series m/e = 43, 57, 71…, which identify linear alkanes, m/e = 41, 55, 69, 83…, which identify alkenes, and characteristic signals of chlorinated hydrocarbons such us those typical for MCM (m/e = 15, 35, 50, 52), DCM (m/e = 49, 51, 84, 86, 88) and TCM (m/e = 35, 41, 47, 58, 83, 85), were detected only in the used catalysts. This supports the hypothesis that the catalysts are poisoned by the production of olefinic complexes and the deposition of (chlorinated) hydrocarbons. Figure 8 shows some of the signals obtained by TGA-MS identifying alkanes and alkenes in the Ru/C catalyst used in the HDC of TCM.

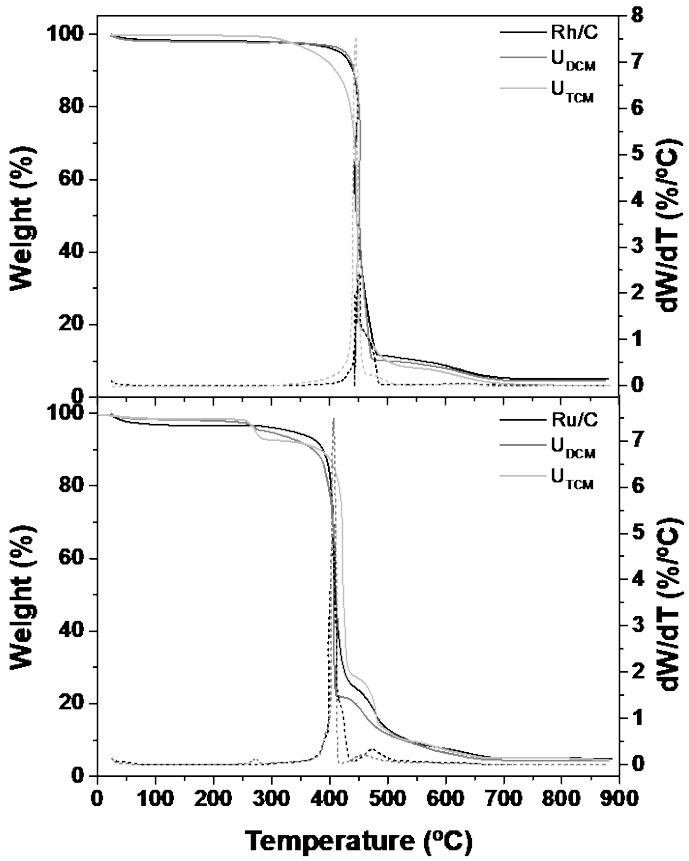

FIGURE 6. Weight loss (solid lines, left axis) during the TGA under air atmosphere of Rh/C and Ru/C before and after use in the HDC reactions, with the corresponding first derivatives (dashed lines, right axis).

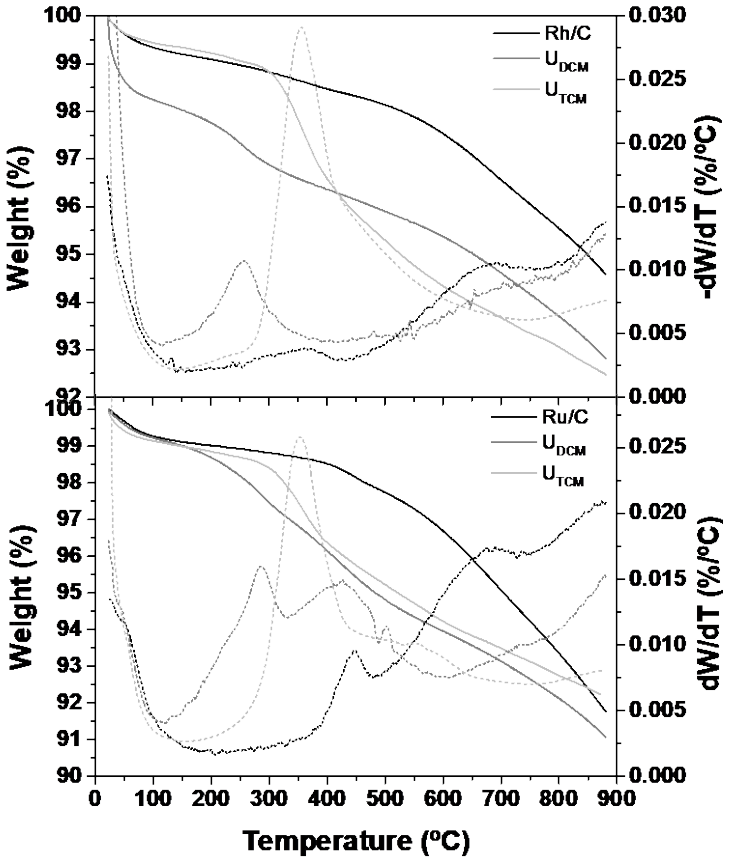

FIGURE 7. Weight loss (solid lines, left axis) during the TGA under inert atmosphere of Rh/C and Ru/C before and after use in the HDC reactions, with the corresponding first derivatives (dashed lines, right axis).

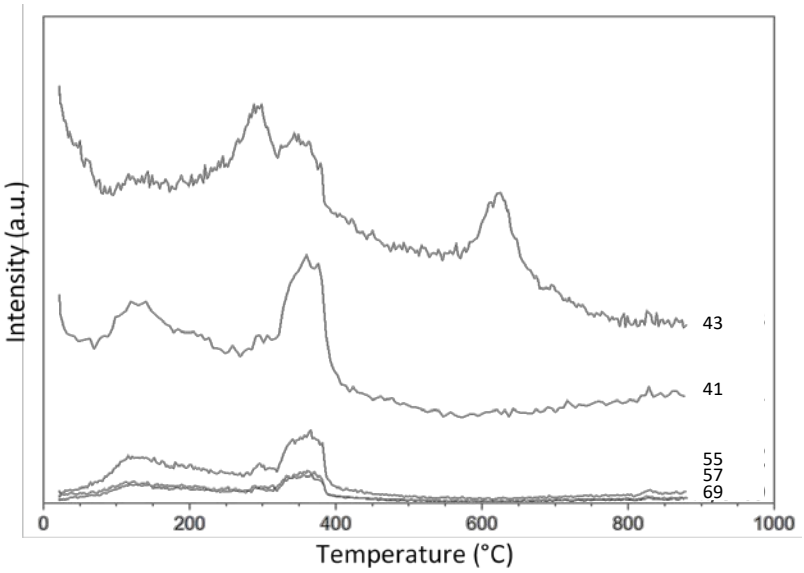

FIGURE 8. Dependence on temperature of selected m/e signals (as indicated) corresponding to alkanes and alkenes evolved during the TGA-MS in inert atmosphere performed on the Ru/C catalyst after use in the HDC of TCM.

In a previous work, the kinetics of the HDC of CMs with Rh/C and Ru/C catalysts were studied [34]. It was found that the HDC of DCM and TCM were well described by the Langmuir-Hinshelwood-Hougen-Watson (LHHW) model with chemical reaction and desorption of reaction products being the rate-controlling steps, respectively. In the HDC of DCM, the lower capacity of these two catalysts, Rh/C and Ru/C, for hydrogenolysis and hydrodechlorination, when compared with similar catalysts prepared with different active phases (*e.g.* Pd/C, Pt/C), explains their reaction step being slower than the adsorption step. That would lead to the formation of a higher diversity of byproducts, as has indeed been observed here (section 3.1). On the other hand, in the HDC of TCM, the overall rate appeared to be determined by the desorption of reaction products. Slow desorption would favour the accumulation of carbonaceous deposits on the catalyst surface, which is consistent with the strong decrease in BET area observed in Table S1 and the weight loss observed in Figure 7 for the used catalysts. Alvarez-Montero et al. [34] considered that different sets of complex reactions may occur on the catalyst surface during the HDC of TCM because of the formation of oligomeric coke-like deposits. This agrees with the hypothesis of the production of new organometallic phases containing chlorine and carbon on the catalyst surfaces.

3.3. Regeneration of the catalysts

Due to the stronger deactivation found for TCM, this reactant was selected as the target feedstock in order to study catalyst regeneration. After each regeneration treatment, the catalysts recovered their activity, being able to convert 100% of TCM, but suffered again a dramatic deactivation with time on stream. Nevertheless, as can be seen in Figure 9, it is remarkable that the selectivity to valuable hydrocarbons (C_{1+} + C_nH_{2n}) increases after each regeneration treatment, particularly for olefins, while selectivity to CH_4 diminishes.

Thus, it seems plausible to use this process, in short deactivation-regeneration cycles, to recycle chloromethanes in order to obtain valuable hydrocarbons.

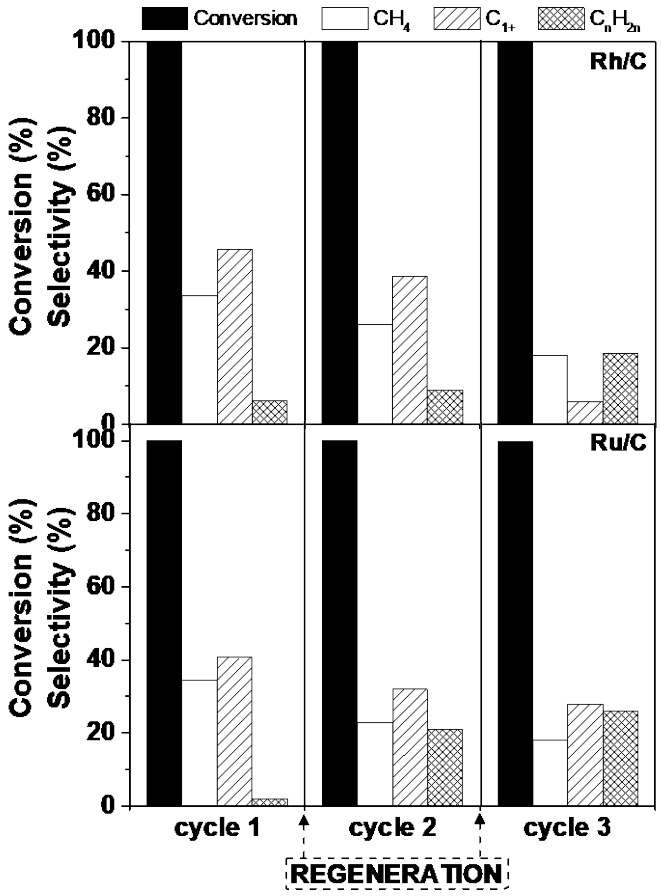

FIGURE 9. Initial conversion of TCM and selectivity to CH_4, other alkanes (C_{1+}) and olefins (C_nH_{2n}) obtained after three consecutive 5-day HDC cycles with Rh/C and Ru/C catalysts.

The characterization of the regenerated catalysts reveals a partial recovery of catalyst porosity after the oxidizing treatment (Table 2), which may be related to the removal of the carbonaceous deposits generated during HDC. The regenerated Rh/C and Ru/C catalysts present a highly microporous nature, with average pore diameters smaller than 1.5 nm (Figure 10).

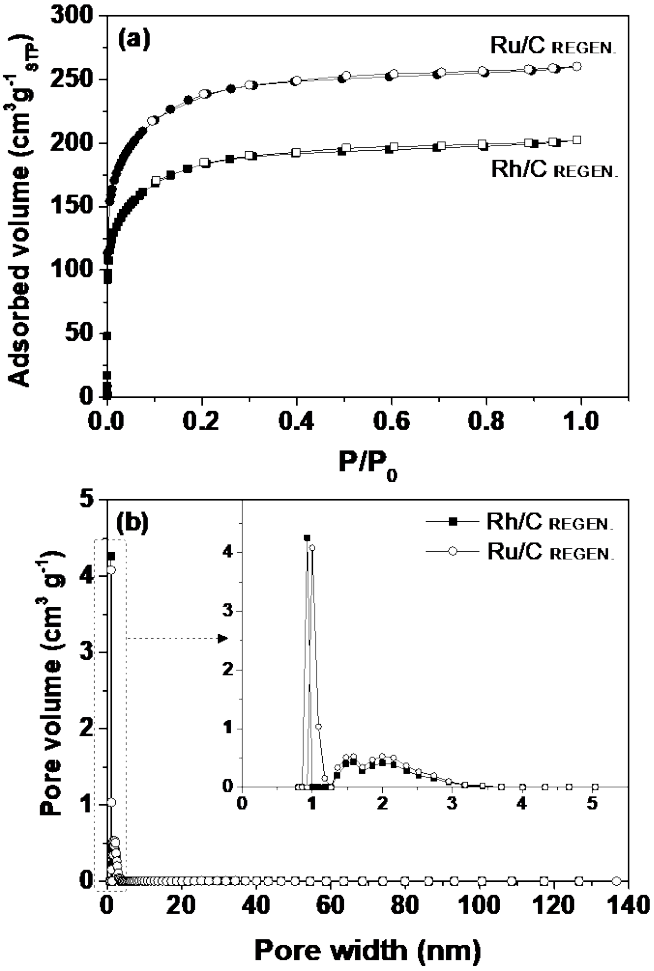

FIGURE 10. N_2 adsorption-desorption isotherms (a) and pore size distributions (b) of the regenerated catalysts.

TABLE 2. Textural and surface composition data for the regenerated Rh/C and Ru/C catalysts.

		Rh/C regen.	Ru/C regen.
S_{BET} (m^2 g^{-1})		616	795
V_{pore} (cm^3 g^{-1})		0.28	0.36
M_{XPS}	M^0 (%)	19.5	-
	M^{n+} (%)	80.5	-
Cl_{XPS}	$Cl_{inorg.}$ (%)	18.1	5.9
	$Cl_{org.}$ (%)	81.9	94.1
C_{XPS}	C=C (%)	56.8	55.7
	C-C (%)	27.1	29.5
	C-O (%)	13.8	10.1
	C=O (%)	2.3	4.7
O_{XPS}	C=O (%)	59.6	47.2
	C-O (%)	30.2	38.5
	O_{ads} (%)	10.2	14.3

TEM images show highly dispersed Rh particles of mean size 2.8 nm (Figure 11); that is, only slightly bigger than those of the as prepared catalyst. By contrast, and as was the case with the Ru catalyst used in the HDC of TCM, metal particles could not be found by TEM in the regenerated Ru/C catalyst.

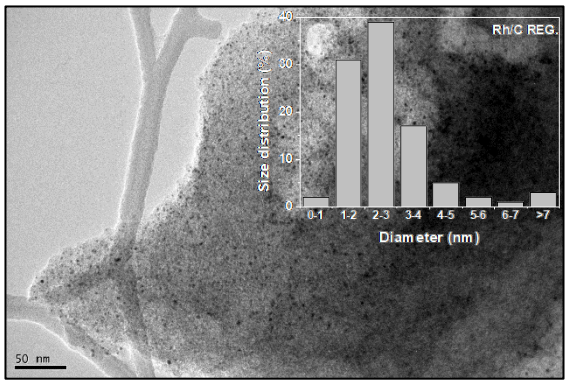

FIGURE 11. TEM image of the regenerated Rh/C catalyst and particle size distribution histogram.

XRD profiles (Figure 12) confirm the absence of large metal particles in both regenerated catalysts. In addition, the signal at 35.4° (#), attributed to the organometallic complexes formed, decreases substantially after the regeneration treatment. To allow direct comparison, XRD patterns of the catalysts used under TCM are included in the figure.

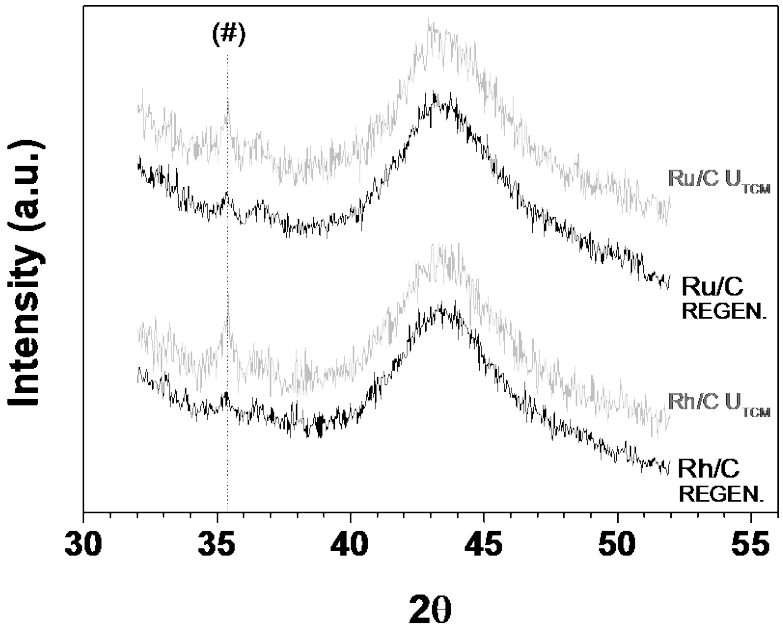

FIGURE 12. XRD profiles of the used and regenerated Rh/C and Ru/C catalysts.

Other changes occurring to the catalyst's surfaces during regeneration, which seem to be key for the recuperation of catalytic activity and for the increased selectivity to valuable hydrocarbons observed, are determined by XPS (Table 2). Although the proportion of Cl_{org} species remains remarkably high for both catalysts, because of the oxidizing nature of the treatment, the concentration of Rh^{n+} species increases to *ca.* 80 %, returning to the initial proportion found in the as prepared catalyst. The same recovery is observed for oxygenated species. The signals attributed to sp^2 and sp^3 carbon species also return to their initial proportions. However, the oxidizing treatment produces an increase in the proportion of epoxy and hydroxyl groups (C-O groups), and does not affect the concentration of carbonyl, carboxyl and carboxylate groups (C=O groups). Therefore, the proportions of these groups in the original and regenerated catalysts are different: the regenerated catalysts contain higher concentrations of epoxy and hydroxyl groups, and lower concentrations of carbonyl, carboxyl and carboxylate groups than the original

catalysts. The different distribution of oxygenated groups seems to be the cause of the different selectivities observed between the original and regenerated catalysts. In a previous study [21], the reaction scheme for the HDC of TCM with Rh/C and Ru/C catalysts was elucidated, showing that olefins are intermediate products in HDC, and that these may be hydrogenated to the corresponding saturated hydrocarbons. The presence of C=O surface groups seem to favour the hydrogenation of olefins to paraffins, whilst C-O groups have lower hydrogenation ability. Thus, when using the regenerated catalysts, which contain a higher proportion of C-O groups, the selectivity to olefins increases. By contrast, when using the original catalyst, with a higher concentration of C=O groups, the intermediate olefins may be hydrogenated, so increasing the selectivity to saturated hydrocarbons.

4. Conclusions

Rh/C and Ru/C catalysts showed high initial activities in the HDC of chloromethanes, but different stability depending on the metal and reactant involved. Rh/C lost only 15% of its activity after 90 h in the HDC of DCM, while during the HDC of TCM the same catalyst suffer a severe deactivation, losing 75% of activity in 84 h. The deactivation of Ru/C is even more dramatic, it losing 75% of activity in *ca.* 55 h in both HDC reactions. The severe deactivation observed is attributed to the formation of new organometallic complexes, which block the pore structure. In addition, metallic sintering is observed in Ru/C during the HDC of DCM. The higher resistance to deactivation observed in Rh/C during the HDC of DCM may be attributed to the migration of Rh particles to the catalyst surface, becoming more accessible for the reaction, and the lower chlorine concentration available for the oligomerization reactions in this case. A regeneration treatment with air at 250 °C successfully recovers the initial activity of these catalysts. Due to the changes

in the surface chemistry of the catalyst, after each deactivation-regeneration treatment, the selectivity to valuable olefins increases. These catalysts and the regeneration procedure described therefore provide a promising route for the upgrading of waste chloromethanes to light olefins, using this process in short deactivation-regeneration cycles.

Acknowledgements

The authors gratefully acknowledge financial support from FEDER/Ministerio de Ciencia, Innovación y Universidades-Agencia Estatal de Investigación/CTM2017-85498-R. M. Martín Martínez acknowledges a postdoctoral grant, 2017-T2/AMB-5668, from the Comunidad de Madrid "Atracción de talento investigador" programme. Electron microscopy was performed at the Electron Microscope Facility, University of St Andrews and at ICTS Centro Nacional de Microscopía Electrónica, Universidad Complutense de Madrid.

References

1. B. Huang, C. Lei, C. Wei, G. Zeng, Chlorinated volatile organic compounds (Cl-VOCs) in environment – sources, potential human health impacts, and current remediation technologies, Environ. Intern. 71 (2014) 118-138.

2. Regulation (EC) No 166/2006 of the European Parliament and of the Council of 18 January 2006.

https://eur-lex.europa.eu/legal-content/HR/TXT/?uri=CELEX:32006R0166 (accessed 30 April 2020).

3. Agency for Toxic Substances & Disease Registry. Toxic Substances Portal – Methylene Chloride.

https://www.atsdr.cdc.gov/toxfaqs/tf.asp?id=233&tid=42 (accessed 30 April 2020).

4. Agency for Toxic Substances & Disease Registry. Toxic Substances Portal – Chloroform.

https://www.atsdr.cdc.gov/ToxProfiles/tp.asp?id=53&tid=16 (accessed 30 April 2020).

5. M. Hu, Y. Liu, Z. Yao, L. Ma, X. Wang, 2017. Catalytic reduction for water treatment. Front. Environ. Sci. Eng., 12(1), 3.

6. F.J. Urbano, J.M. Marinas, Hydrogenolysis of organohalogen compounds over palladium supported catalysts, J. Mol. Catal. A-Chem. 173 (2001) 329-345.

7. V.I. Simagina, O.V. Netskina, E.S. Tayban, O.V. Komova, E.D. Grayfer, A.V. Ischenko, E.M. Pazhetnov, The effect of support properties on the activity of Pd/C catalysts in the liquid-phase hydrodechlorination of chlorobenzene, Appl. Catal. A-Gen. 379 (2010) 87-94.

8. N.C. Concibido, T. Okuda, W. Nishijima, M. Okada, Deactivation and reactivation of Pd/C catalyst used in repeated batch hydrodechlorination of PCE, Appl. Catal. B-Environ. 71 (2007) 64-69.

9. P. Forni, L. Prati, M. Rossi, Catalytic dehydrohalogenation of polychlorinated biphenyls Part II: Studies on a continuous process, Appl. Catal. B-Environ. 14 (1997) 49-53.

10. S. Ordonez, F.V. Diez, H. Sastre, Characterisation of the deactivation of platinum and palladium supported on activated carbon used as hydrodechlorination catalysts, Appl. Catal. B-Environ. 31 (2001) 113-122.

11. B. Aristizabal, C.A. Gonzalez, I. Barrio, M. Montes, C.M. de Correa, Screening of Pd and Ni supported on sol-gel derived oxides for dichloromethane hydrodechlorination, J. Mol. Catal. A-Chem. 222 (2004) 189-198.

12. C.H. Bartholomew, Mechanisms of catalyst deactivation, Appl. Catal. A-Gen. 212 (2001) 17-60.

13. B. Coq, J.M. Cognion, F. Figueras, D. Tournigant, Conversion under hydrogen of dichlorodifluoromethane over supported palladium catalysts, J. Catal. 141 (1993) 21-33.

14. S.Y. Kim, H.C. Choi, O.B. Yanga, K.H. Lee, J.S. Lee, Y.G. Kim, Hydrodechlorination of tetrachloromethane over supported Pt catalysts, J. Chem. Soc. - Chem. Commun. (1995) 2169-2170.

15. D.J. Moon, M.J. Chung, K.Y. Park, S.I. Hong, Deactivation of Pd catalysts in the hydrodechlorination of chloropentafluoroethane, Appl. Catal. A-Gen. 168 (1998) 159-170.

16. A.G.F. de Souza, A.M.P. Bentes, A.C.C. Rodrigues, L.E.P. Borges, J.L.F. Monteiro, Hydrodechlorination of carbon tetrachloride over PtNaX zeolite: Deactivation studies, Catal. Today 107-108 (2005) 493-499.

17. S. Liu, M. Martin-Martinez, A.M. Álvarez-Montero, A. Arevalo-Bastante, J.J. Rodriguez, M.L. Gómez-Sainero, Recycling of gas phase residual dichloromethane by hydrodechlorination: Regeneration of deactivated Pd/C catalysts, Catalysts 9 (2019).

18. E. Lopez, S. Ordonez, F.V. Diez, Deactivation of a Pd/Al_2O_3 catalyst used in hydrodechlorination reactions: Influence of the nature of organochlorinated compound and hydrogen chloride, Appl. Catal. B-Environ. 62 (2006) 57-65.

19. S. Ordonez, H. Sastre, F.V. Diez, Hydrodechlorination of tetrachloroethene over Pd/Al_2O_3: Influence of process conditions on catalyst performance and stability, Appl. Catal. B-Environ. 40 (2003) 119-130.

20. D.A. Dodson, H.F. Rase, Methylene Chloride from chloroform by hydrochlorination, Ind. Eng. Chem. Prod. Res. Dev. 17 (1978) 236-240.

21. M. Martin-Martinez, L.M. Gomez-Sainero, M.A. Alvarez-Montero, J. Bedia, J.J. Rodriguez, Comparison of different precious metals in activated carbon-supported catalysts for the gas-phase hydrodechlorination of chloromethanes, Appl. Catal. B-Environ. 132 (2013) 256-265.

22. M. Martin-Martinez, A. Alvarez-Montero, L.M. Gomez-Sainero, R.T. Baker, J. Palomar, S. Omar, S. Eser, J.J. Rodriguez, Deactivation behavior of Pd/C and Pt/C catalysts in the gas-phase hydrodechlorination of chloromethanes: Structure-reactivity relationship, Appl. Catal. B-Environ. 162 (2015) 532-543.

23. A. Arevalo-Bastante, M. Martin-Martinez, A.M. Álvarez-Montero, J.J. Rodriguez, M.L. Gómez-Sainero, Properties of carbon-supported precious metals catalysts under

reductive treatment and their influence in the hydrodechlorination of dichloromethane, Catalysts 8 (2018).

24. M.A. Alvarez-Montero, L.M. Gomez-Sainero, A. Mayoral, I. Diaz, R.T. Baker, J.J. Rodriguez, Hydrodechlorination of chloromethanes with a highly stable Pt on activated carbon catalyst, J. Catal. 279 (2011) 389-396.

25. L.M. Gómez-Sainero, J. Palomar, S. Omar, C. Fernández, J. Bedia, A. Álvarez-Montero, J.J. Rodriguez, Valorization of chloromethanes by hydrodechlorination with metallic catalysts, Catal. Today 310 (2018) 75-85.

26. T.F. Garetto, C.I. Vignatti, A. Borgna, A. Monzón, Deactivation and regeneration of Pt/Al_2O_3 catalysts during the hydrodechlorination of carbon tetrachloride, Appl. Catal. B-Environ. 87 (2009) 211-219.

27. M. Legawiec-Jarzyna, A. Srebowata, W. Juszczyk, Z. Karpinski, Hydrodechlorination of dichlorodifluoromethane, carbon tetrachloride and 1,2-dichloroethane over Pt/Al_2O_3 catalysts, J. Mol. Catal. A-Chem. 224 (2004) 171-177.

28. B. Heinrichs, F. Noville, J. Schoebrechts, J. Pirard, Palladium-silver sol-gel catalysts for selective hydrodechlorination of 1,2-dichloroethane into ethylene. IV. Deactivation mechanism and regeneration., J. Catal. 220 (2003) 215-225.

29. C.A. Gonzalez, M. Bartoszek, A. Martin, C.M. de Correa, Hydrodechlorination of light organochlorinated compounds and their mixtures over Pd/TiO_2-washcoated minimonoliths, Ind. Eng. Chem. Res. 48 (2009) 2826-2835.

30. S. Ordonez, E. Diaz, F.V. Diez, H. Sastre, Regeneration of Pd/Al2O3 catalysts used for tetrachloroethylene hydrodechlorination, React. Kinet. Catal. L. 90 (2007) 101-106.

31. M. Bonarowska, Z. Kaszkur, L. Kępiński, Z. Karpiński, Hydrodechlorination of tetrachloromethane on alumina- and silica-supported platinum catalysts, Appl. Catal. B-Environ. 99 (2010) 248-256.

32. E. Diaz, A.F. Mohedano, J.A. Casas, J.J. Rodriguez, Analysis of the deactivation of Pd, Pt and Rh on activated carbon catalysts in the hydrodechlorination of the MCPA herbicide, Appl. Catal. B-Environ. 181 (2016) 429-435.

33. C.D. Wagner, L.E. Davis, M.V. Zeller, J.A. Taylor, R.H. Raymond, L.H. Gale, Empirical atomic sensitivity factors for quantitative analysis by electron spectroscopy for chemical analysis, Surf. Interface Anal. 3 (1981) 211-225.

34. M.A. Álvarez-Montero, M. Martin-Martinez, L.M. Gómez-Sainero, A. Arevalo-Bastante, J. Bedia, J.J. Rodriguez, Kinetic study of the hydrodechlorination of chloromethanes with activated-carbon-supported metallic catalysts, Ind. Eng. Chem. Res. 54 (7) (2015) 2023-2029.

35. M. Bonarowska, Z. Karpiński, Hydrodechlorination of tetrachloromethane over supported platinum catalysts. Effects of hydrogen partial pressure and catalyst's screening protocol on the catalytic performance, Top. Catal. 55 (2012) 846-852.

36. E.J. Creyghton, M.H.W. Burgers, J.C. Jansen, H. van Bekkum, Vapor-phase hydrodehalogenation of chlorobenzene over platinum/H-BEA zeolite, Appl. Catal. A-Gen. 128 (1995) 275-288.

37. M.A. Alvarez-Montero, L.M. Gomez-Sainero, J. Juan-Juan, A. Linares-Solano, J.J. Rodriguez, Gas-phase hydrodechlorination of dichloromethane with activated carbon-supported metallic catalysts, Chem. Eng. J. 162 (2010) 599-608.

38. J.F. Moulder, W.F. Stickle, P.E. Sobol, K.D. Bomben, Handbook of X-ray photoelectron spectroscopy: A reference book of standard data for use in X-ray photoelectron spectroscopy, Physical Electronics Division, Perkin-Elmer Corp.

39. M.V. Pagliaro, M. Bellini, M. Bevilacqua, J. Filippi, M.G. Folliero, A. Marchionni, H.A. Miller, W. Oberhauser, S. Caporali, M. Innocenti, F. Vizza, Carbon supported Rh nanoparticles for the production of hydrogen and chemicals by the electroreforming of biomass-derived alcohols, RSC Adv. 7 (2017) 13971-13978.

40. L.S. Kibis, A.I. Stadnichenko, S.V. Koscheev, V.I. Zaikovskii, A.I. Boronin, XPS Study of Nanostructured Rhodium Oxide Film Comprising Rh^{4+} Species, J. Phys. Chem. C 120 (2016) 19142-19150.

41. M. Carvalho, L.F. Wieserman, D.M. Hercules, Spectroscopic characterization of Wilkinson's catalyst using X-ray photoelectron spectroscopy (ESCA), Appl. Spectrosc. 36 (1982) 290-296.

42. Z.M. Michalska, M. Čapka, J. Stoch, Silica-supported rhodium complexes. Relation between catalyst structure and activity, J. Mol. Catal. 11 (1981) 323-330.

43. M.A. Garralda, L. Ibarlucea, Tetraphenylborate tetra- and pentacoordinated Complexes of rhodium(I) with diolefins, Polyhedron 1 (1982) 339-341.

44. M. Gregori, G. Fornasari, G. Marchionni, V. Tortelli, S. Millefanti, S. Albonetti, Hydrogen-assisted dechlorination of $CF_3OCFCl–CF_2Cl$ to $CF_3OCF=CF_2$ over different metal-supported catalysts, Appl. Catal. A-Gen. 470 (2014) 123-131.

45. D. Luo, G. Zhang, J. Liu, X. Sun, Evaluation criteria for reduced graphene oxide, J. Phys. Chem. C 115 (2011) 11327-11335.

46. M.K. Brown, E.J. Corey, Catalytic enantioselective formation of chiral-bridged dienes which are themselves ligands for enantioselective catalysis, Org. Lett. 12 (2010) 172-175.

47. R. Shintani, K. Ueyama, I. Yamada, T. Hayashi, Chiral norbornadienes as efficient ligands for the rhodium-catalyzed asymmetric 1,4-addition of arylboronic acids to fumaric and maleic compounds, Org. Lett. 6 (2004) 3425-3427.

48. U. Florke, U. Ortmann, H. Haupt, Rhodium(i) cyclooctadiene (cod) complexes with the *N*-donor ligands 1,8-diazabicyclo[5.4.0]undec-7-ene (dbu) and 1,5-diazabicyclo[4.3.0]non-5-ene (dbn), Acta Crystallogr. Sect. C-Cryst. Struct. Commun. 48 (1992) 1663-1665.

49. S. Kim, G.Y. Lee, J. Baeg, Y. Kim, S. Kim, J. Kim, Visible-light-driven photoproduction of hydrogen using rhodium catalysts and platinum nanoparticles with formate, J. Phys. Chem. C 118 (2014) 25844-25852.

50. K.A. Abboud, J. Yin, W. Jones, Carbonylchloro(η^5-cyclopentadienyl)(1-ethoxybutylidene)ruthenium, Acta Cryst. C 53 (1997) IUC9700011-IUC9700011.

51. C.K. Chung, R.H. Grubbs, Olefin metathesis catalyst: Stabilization effect of backbone substitutions of N-heterocyclic carbene, Org. Lett. 10 (2008) 2693-2696.

52. C.D. Taboada, J. Batista, A. Pintar, J. Levec, Preparation, characterization and catalytic properties of carbon nanofiber-supported Pt, Pd, Ru monometallic particles in aqueous-phase reactions, Appl. Catal. B-Environ. 89 (2009) 375-382.